Acquisition and Pointing for Mars Optical Access Link

Martin Regehr, Joseph Kovalik, Abhijit Biswas
Jet Propulsion Laboratory
California Institute of Technology
4800 Oak Grove Drive, Pasadena, CA 91109
818-393-1203
Martin.W.Regehr@jpl.nasa.gov

Abstract—Optical characteristics can potentially benefit "access" links at Mars when transmitting data from surface to orbiting assets because of the higher gain and modulation bandwidth, compared to radio frequency (RF). Furthermore, higher bits/kg/W can be realized with low mass and power optical systems, enabling the streaming of high definition imagery. In this paper we present a conceptual design for a low complexity, autonomous optical communications link for returning data at 50-200 Mb/s from the Martian surface and for lower forward data rates of 50 kb/s to the surface. The pointing control is simplified by widening the transmitted laser beams (0.5 – 2.0 mrad) for the short distance (400-1200 Km) links. Link acquisition is based on the orbiter transceiver (OT) "blind"-pointing a laser beam to illuminate the lander transceiver (LT) on the surface. The LT acquires the link with a spectrally-filtered wide-field-of-view camera and subsequently tracks the orbiter transceiver with a two-axis, stepper-motor-actuator, to send back a laser modulated with high-rate data to the orbiting asset. The system design also has a provision for the OT transitioning from blind-pointing to closed loop tracking once it acquires the signal from the lander transceiver. Results from successful ground-based demonstrations performed at JPL, in which the pointing rate required to track an orbiter was emulated by mounting both transceivers on rotating stages, and in which we transmitted live video and pseudo-random data streams, are presented.

TABLE OF CONTENTS

1. INTRODUCTION.....1
2. LINK ANALYSIS.....1
3. TRANSCEIVER DESIGN & PROTOTYPING.....4
4. PROTOTYPE LINK.....8
5. CONCLUSION.....9
ACKNOWLEDGEMENTS..... 10
REFERENCES.....10
BIOGRAPHY.....10

1. INTRODUCTION

Communication with spacecraft used for planetary exploration remains one of the key factors limiting the capabilities of such missions. Recently deployed communication links from the surface of Mars, for example, have delivered mean data rates of 0.250-1 Gb/sol using UHF transmission from the Martian surface (Mars Exploration Rovers and Phoenix) to orbiting spacecraft such a the Mars Odyssey and the Mars Reconnaissance Orbiter (MRO). We show that an optical relay link from the Martian surface to an orbiter in a 300-400 km circular orbit is capable of returning 50-100 Gb/sol. This exceeds by almost an order of magnitude the expected UHF returns from the Mars Science Laboratory (MSL).

A key technical challenge [1] for a Martian optical access link is the dust-laden Mars atmosphere which can cause severe signal attenuation and contribute to background noise by scattering of sunlight. We have modeled the Mars atmospheric attenuation and scattering characteristics and obtained favorable agreement with measurements made by Mars missions such as Viking, MER and the Mars Observer Laser Altimeter (MOLA). These results will be reported elsewhere, but we have used the results in the link analysis reported here.

Acquisition and pointing is always challenging for laser links, to be a viable replacement for the simple UHF links in use today, any candidate optical link must both acquire lock and operate autonomously. The relatively short distance covered by the access link makes it possible to use a wider beam while still delivering a desired irradiance to a remote receiver, however, and the use of wider beams simplifies the pointing problem. We believe that robust solutions to these challenges, with mass and power consumption comparable to those of currently used UHF links, will make a very strong case for implementing optical links in future Mars missions. Moreover, the case will likely be of equal merit at the Moon, especially for supporting the human missions planned in the next decade.

In section 2 below we describe the concept of operations, with link analysis for the most difficult wide-angle link acquisition. In section 3 the transceiver designs that were prototyped for testing are described. Results of end-to-end link emulation are discussed in section 4, and conclusions are presented in section 5.

2. LINK ANALYSIS

The concept of operations we are pursuing for autonomous acquisition presumes that both the position and attitude of

1

[1]Copyright 2008 California Institute of Technology.
Government sponsorship acknowledged.

the orbiter are precisely known, from ranging measurements and from a star tracker on the orbiter, respectively. The lander's position is well known from ranging prior to landing, from any prior optical contact with the lander, and from its low maximum velocity, if it is capable of moving at all. The lander's attitude, however, may have uncertainties of several degrees in both elevation and azimuth.

Pointing acquisition proceeds in four phases. First, the orbiter transceiver, using "blind" pointing based on knowledge of the orbiter position and attitude, and knowledge of the lander's position, illuminates the lander transceiver.

Second, the lander transceiver detects the beam from the orbiter transceiver, and the lander transceiver telescope is aimed at the orbiter transceiver. To detect the orbiter transceiver beam, the lander transceiver employs a wide-field-of-view (WFOV) camera. Because other bright objects will be in the WFOV camera's field of view, the camera uses both an optical filter and motion detection to reject sources other than the beacon transmitted by the orbiter transceiver. The optical filter is a narrow (~ 1 to 2 nm) bandpass filter centered on the orbiter transceiver's laser wavelength. Motion detection is done using a moving-difference filter, i.e., consecutive exposures taken by the WFOV camera are subtracted, so that in the difference image, stationary or slowly-moving objects are nearly invisible. In the filter output, the beacon from the relatively fast-moving lander produces a large amplitude negative spot at the location it occupied in the first of a pair of images and a large positive spot at its location in the second image; these peaks are identified by an appropriate algorithm in the LT.

Third, once the orbiter transceiver's beacon is in the field of view of the lander transceiver's pointing detector, control of the lander transceiver's telescope pointing gimbal is transferred from the WFOV camera to the pointing detector. This establishes pointing lock in the lander transceiver, and allows the lander transceiver to point with sufficient accuracy to illuminate the orbiter transceiver.

Finally, when the orbiter transceiver detects the beam transmitted by the lander transceiver, control of the orbiter transceiver's telescope pointing gimbal is transitioned from a blind pointing mode to a closed-loop mode in which pointing is controlled by the error signal from the pointing detector. Received photon flux λ_s is generally given by:

$$\lambda_s = P_0 G_T \eta_T \eta_{Strehl} L_P L_{space} \eta_{Mars_atmos} G_R \eta_R \left(\frac{hc}{\lambda_{OT}} \right) \quad (1)$$

P_0 is the average laser power output by the OT transmitter,
G_T transmitter gain,
η_T is transmitter efficiency,
η_{Strehl} is the Strehl efficiency of the laser transmitter,
L_p is the net loss due to mis-pointing of the transmitted laser beam,
L_{space} is the space-loss term,
η_{Mars_Atmos} is Mars atmospheric attenuation,
G_R is the receiver gain,
η_R is the receiver efficiency,
h is Planck's constant,
c is velocity of light,
λ_{OT} is the OT laser transmitter wavelength.

G_T, the transmitter gain is estimated for a fiber laser coupled to a lens assembly with an effective exit aperture diameter D_T, by Eq. (2)

$$G_T = \left[\frac{\pi D_T}{\lambda_{OT}} \right]^2 \quad (2)$$

η_T is the optical transmittance of the lens assembly and η_{Strehl} is an allocation meant to account for the combined Strehl imperfections of the exiting laser beam, as well as, scattering losses.

The pointing-loss L_p is an allocation in the photon-budget. In section 4.1.2 dependencies on beam-width and pointing mechanisms related to L_p are further elaborated.

The wavelength normalized space loss, L_s, is given by:

$$L_s = \left[\frac{\lambda_{OT}}{4\pi R} \right]^2 \quad (3)$$

where R represents the range from the OT to the LT. During the time that line-of-sight exists between the orbiter and the lander, L_s and η_{Mars_Atmos} will vary continuously because of the varying range and the zenith angle dependence of the atmospheric attenuation. A summary of the Mars atmospheric attenuation using Spectral Mapping Atmospheric Radiative Transfer (SMART) at 810 nm and 1064 nm is shown in Figure 1 below.

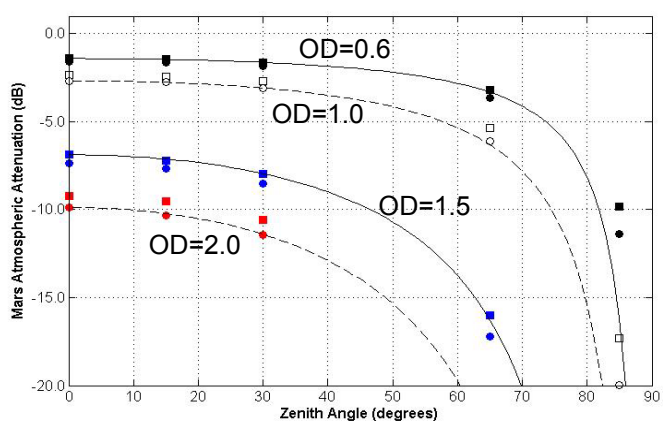

Figure 1 Summary of Mars atmospheric attenuation at 810 nm (squares) and 1064 nm (circles) corresponding to optical depths at 500 nm shown on the secant fits (lines) to the data.

TABLE 1 Summary of downlink parameters

Laser wavelength (mm)	0.81
Beam Divergence (mrad)	600
Laser Energy (dBW)	0.00
Transmitter Gain (dB)	73.55
Tranmsitter Loss (dB)	-0.13
Strehl Loss (dB)	-1.55
Pointing Loss (dB)	-3.50
Receiver Gain (dB)	83.66
Receiver Efficiency (dB)	-3.01

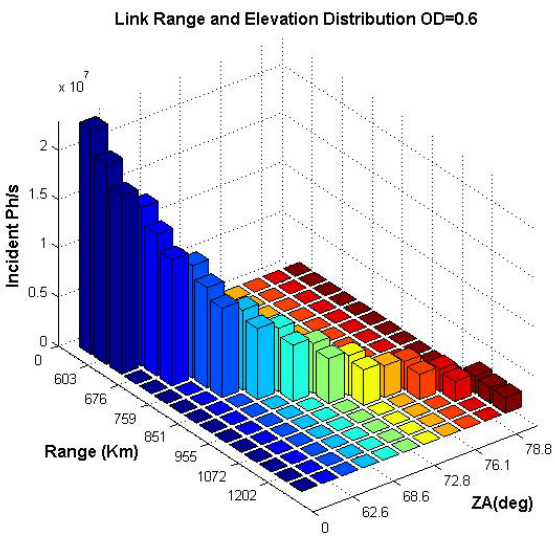

(a)

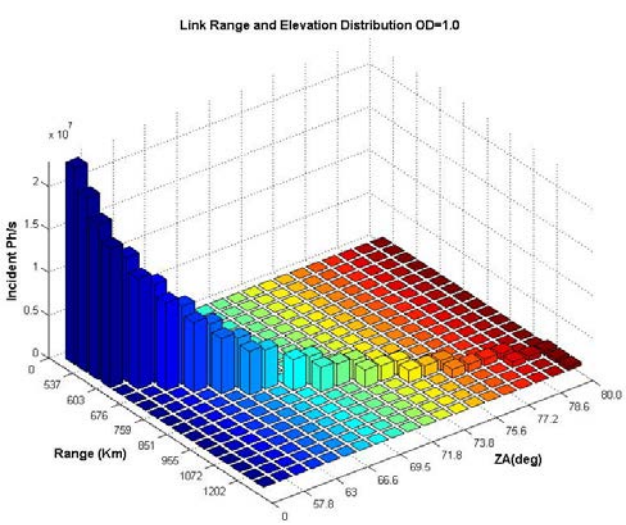

(b)

Figure 2 Incident photon flux (ph/s) corresponding to (a) OD=0.6 and (b) OD=1.0

The attenuation through the Martian atmosphere varies with time of year and local conditions [1] but is lower than OD=1.0 most of the time. In this paper we show some examples corresponding to attenuations expected at OD 0.6 and 1.0.

The Satellite Orbital Analysis Program (SOAP) was used to simulate a spacecraft orbiting Mars at an altitude of 400 Km and an inclination of 75° with a landed asset at the equator. Link parameters such as range, zenith angles and Sun angles were output for one month's duration. The SOAP output file was processed with a MATLAB script to estimate the signal photon flux (Equation 1) incident on the LT using the parameters listed in Table 1.

Figure 2 shows the received photon flux as a function of range and zenith angle for two different assumptions about atmospheric attenuation. The optical density ("OD") of the atmosphere is defined as the base-10 logarithm of the power loss for light transmitted vertically through the atmosphere.

Although the WFOV camera lens has a diameter of 30 cm, its effective aperture is only 3.8 mm. This is because the lens deviates significantly from a paraxial lens: when light reaches the lens from a distant source near the horizon, parts of the lens are shaded by the lens itself, and parts of the illuminated region of the lens are unable to redirect incident rays onto the detector.

Background noise will limit the signal-to-noise ratio (SNR). A WFOV optical system that views an annular region of the sky extending from 10° - 40°elevation angle is appropriate because acquisition will usually occur a large zenith angles. Figure 3 below shows a schematic view of such an acquisition system.

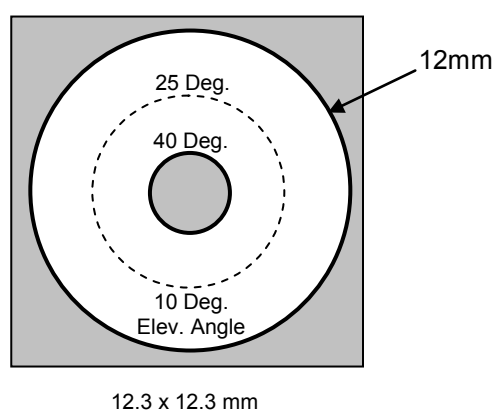

Figure 3 Wide-angle acquisition scheme that views an annular region of sky covering 10° - 40° elevation and images it over a 12-mm diameter.

The solid angle of the annular portion is given by Equation

4:

$$\Omega_{tot} = 2\pi[1-\cos(90-\theta_{low})] - 2\pi[1-\cos(90-\theta_{high})] \quad (4)$$

Where θ_{low} and θ_{high} represent the lower and higher elevation angles. The illuminated circle area in Figure 3 is 65% of the square focal plane area. Table 2 lists the camera characteristics presumed. The background over a 7 x 7 pixel region (slightly larger than the spot size), assuming a 2nm narrow bandpass filter and worst case sky radiance (10 degrees from the sun) of 300 W/m^2/sr/µm. [2] was computed and is shown in Figure 4 along with the weakest detected signal estimates for OD=10.6 and OD=1.0.

Table 2

Focal Plane APS Chip Format	1024 x 1024
Pixel Pitch (µm)	12
QE at 810 nm	0.20
Dark Current (pA/cm^2)	153
Read Noise (e$^-$/pixel/frame)	16
Full Well Depth (electrons)	388, 000

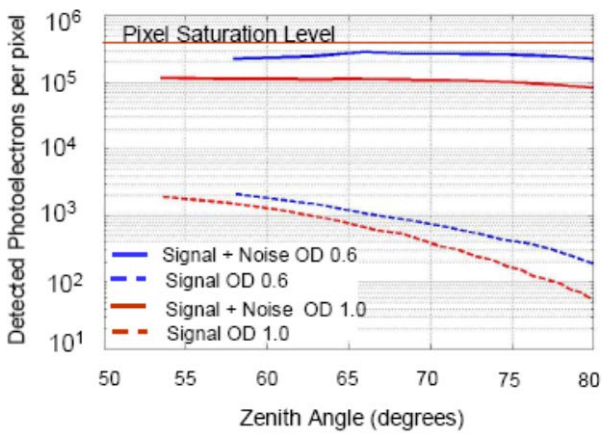

Figure 4 summary of estimated signal and noise detected per pixel on the WFOV camera

The exposure times used for the OD =0.6 and OD =1.0 cases were 10ms and 30 ms, respectively.

Operationally the WFOV camera will use a moving difference filter so that for each pair of subtracted frames a √2 enhancement in SNR will be encountered. Using a Neyman-Pearson decision rule [3] high probability of detection (> 0.99999) with low probability of false alarm < 1E-8) could be achieved with 8 or less frames of acquired data under the worst case conditions.

The WFOV camera acquisition is most stressing given the combination of small entrance aperture diameter and very wide filed of view. Other elements of the link operate with larger area optics and smaller FOVs, the photon budgets for closing these links and accomplishing the high-rate communications will be reported in a future report.

During each 120 minute orbit, the orbiter is in view of the lander for varying lengths of time varying from 3-13 minutes while the range varies from 400-1200 Km.

Uplink

Because science data, especially those containing high-resolution images, can be voluminous, the return or uplink from the LT to the OT benefits particularly from the use of an optical link. Based on the SOAP simulations a very conservative estimate based on 40 passes with an average duration of 10-minutes and an average instantaneous data rate of 50 Mb/s yields data volumes of 40 Gb/sol. A factor of 2-4 higher than this conservative estimate can easily be expected.

A 1 W laser in the LT, transmitted in a 0.7 mrad wide beam, and received through a 6 cm aperture telescope at the OT over a 1000 km range, will result in photon fluxes of 6 x10^8 ph/s incident on the OT data detector accounting for 10-dB of atmospheric attenuation and other reasonable losses. With a photon-counting detector data rate of 50 Mb/s can easily be satisfied at these signal levels even in the presence of expected upwelling radiance background levels at Mars.

Downlink

Both because of the high cost of delivering mass to the Martian surface, and because the data rate needed to send commands to the lander is low, the LT uses a substantially smaller telescope, with a diameter of 2.2 cm. The OT transmits 1 W of laser (see Table 1) more than sufficient for data rates of 50 - 500 kb/s. We anticipate transmitting data at average data rates of 100 kb/s, so that error rates should be low, even after imperfections such as dust in the atmosphere and on the optics, and imperfect pointing, are taken into account.

3. TRANSCEIVER DESIGN AND PROTOTYPING

Figure 5 shows an overview of the operations concept. The access link OT is on board a spacecraft orbiting Mars while the LT, comprising a WFOV camera and separate gimbaled transceiver is on a Mars surface asset.

The orbiter and lander transceiver as currently conceived use a small lens coupled to an optical fiber for transmission, and a significantly larger lens for reception. The transmitter and receiver lenses are co-bore-sighted to each other. To minimize the burden on the lander a larger aperture diameter is chosen for the OT. Additionally, a possible synergy with the optical navigation camera (ONC) that was

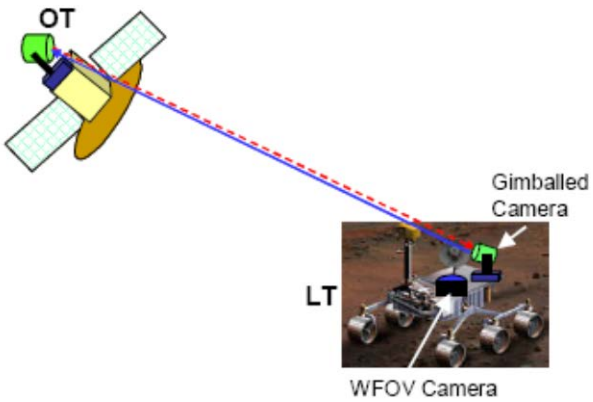

Figure 5 Lander Transceiver (LT) and Orbiter Transceiver (OT)

flown on MRO suggests a design whereby modifications to the MRO ONC would allow reception of returned optical signal from the surface without compromising optical navigation requirements.

TABLE 3 Key design features for OT and LT

	OT	LT
Wavelength Transmitted (nm)	810	1060
Receive Aperture Diameter (mm)	60	22
Wide Angle FOV	NA	(10°-40°) Elevation 360°Azimuth
NavCam FOV	± 0.7°	NA
Tracking Camera FOV (mrad)	0.9	64 x 48
Comm Detector FOV (mrad)	0.5	10
Transmit Beam Divergence (mrad)	0.6	1
Filter Noise Equivalent Bandwidth (NEB)	700-800 nm on NavCam 3-nm on Track and Comm	2-nm for WFOV Cam 3 nm for Gimballed Receiver

The LT WFOV camera design is driven by the link analysis presented in the previous section. A conceptual design for achieving the 3-4 mm diameter entrance aperture with simultaneous narrow band filtering is being pursued. The LT transceiver utilizes a 2.2 cm clear aperture diameter lens with a tracking focal plane array and a detector for receiving forward link. Table 3 lists the key design features for the OT and LT and Figure 6 shows a schematic view of the optical architecture.

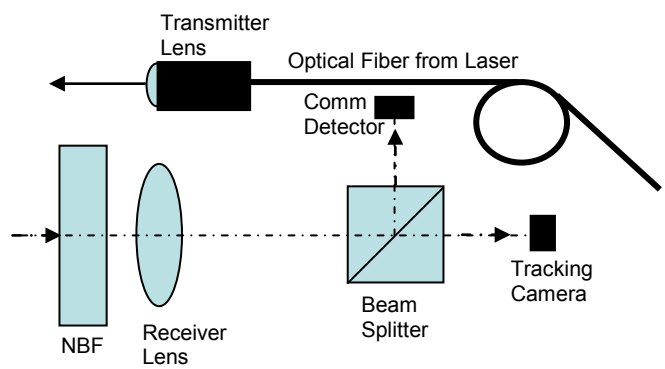

(a)

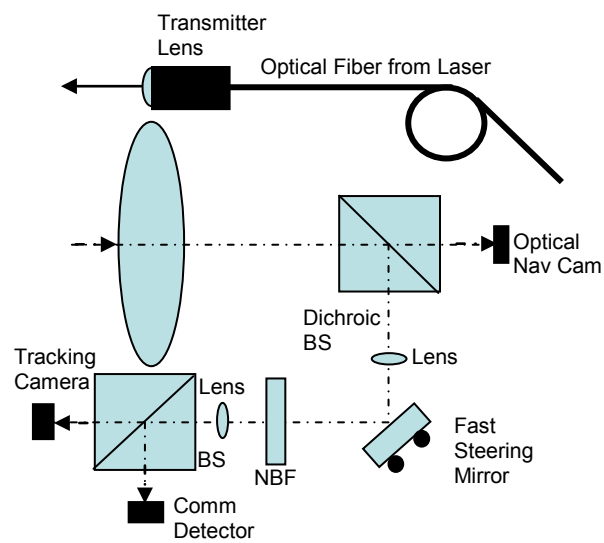

(b)

Figure 6 Optical transciever architecture for (a) LT and (b) OT

Optical designs based on the architectures shown, integrated to two-axis gimbals, sensors and detectors with associated electronics and processors, constitute the designs we propose for flight.

Prototype Lander Transceiver Design

The prototype LT shown schematically in Figure 6a uses a 2.2 cm diameter clear aperture lens with a 25 mm 3-nm wide narrow band filter mounted in front. A silicon CMOS camera Basler Model A601 was used for the tracking sensor. A commercial avalanche photo-diode was used for the communication sensor. The LT laser is a 1060-nm fiber-coupled Lumics laser diode, coupled to a fiber Bragg grating which limits it to single-mode operation and reduces the linewidth of its output. A single mode optical fiber patch cord delivers the laser light to the optical head, which transmits a 2 milliradian beam. This beam divergence exceeds what eventually would be implemented for a Mars access link, but was adopted for prototyping so that using commercially available gimbals and components a viable yet cost-effective system design could be devised for proof-of-concept validation. The laser transmitter can be modulated with streaming video by means of a Serial Digital Interface (SDI) module that outputs a 270 Mb/s signal. Alternatively, a pseudo-random bit sequence (PRBS) generator at 200 Mb/s PN7 was used to modulate the laser.

The optical head of the LT was mounted on a Directed Perceptions D46B two-axis micro-stepper motor gimbal.

The tracking sensor read-out, processing (centroid calculation) and gimbal commanding were performed using a compact PXI crate based processor running real-time LabView.

The WFOV detector in the prototype LT uses a Fujinon 1.8 mm focal-length 1.4 focal ratio fish-eye lens. This commercial lens provides a field of view exceeding 2π steradians: when pointed vertically upwards it is able to image a region extending from straight up to 5 degrees below horizontal. In order to achieve spectral filtering with this lens custom re-collimation optics were integrated with the lens so that the narrow band filter was in a collimated part of the beam. This assembly afforded only a 0.7 mm entrance aperture diameter compared to 3.8 mm used in our analysis in Section 2 and the optical transmission of the overall assembly was 23% compared to 50% assumed in Table 1

The wide field of view lens introduces significant aberrations. As a result, it was necessary to perform a calibration procedure to determine the pointing command which, when sent to the lander transceiver gimbal, would result in the lander transceiver telescope pointing at an object identified in the acquisition camera image as the orbiter transceiver beacon.

This calibration was done by setting up the lander transceiver prototype in a reflective half-dome, onto the interior of which we projected a laser spot. A control loop was closed around the pointing detector and the gimbal in the prototype lander transceiver, so that the gimbal would follow any motion of the laser spot. The spot was then moved to a range of positions on the interior of the dome, and gimbal position was recorded together with the laser spot coordinates measured simultaneously in the acquisition camera. A two-dimensional fitting routine was then used to determine the coefficients in a mapping from pixel coordinates in the acquisition camera to azimuth and elevation angles in the lander transceiver gimbal. Figure 7 shows a photograph of the lander transceiver assembly.

Prototype Orbiter Transceiver Design

The prototype orbiter transceiver uses a 6.9 cm aperture diameter commercial lens with a focal length of 500mm as a receiving telescope. The navigation camera and tracking sensor utilize Basler Model A601 silicon CMOS cameras. A Perkin Elmer Model C30659-1060-R8BH avalanche photodiode (APD) was used as the data detector. The FOV of the Navigation camera channel was $\pm$ 0.5 degrees. A 100-nm bandpass filter (700-800 nm) was used in front of the Navigation camera. During testing light emitting diodes (LED's) matching this bandpass can be used to assist acquisition. The tracking and communication data detector channels utilize 3-nm wide optical filters centered at 1060 nm (see Foigure 6b).

A single-mode fiber-coupled diode laser operating at 808 nm was used as the transmitter. A 50-Kb/s data stream generated by a low rate PRBS generator was modulated on this laser. The laser beamwidth transmitted from the OT is also 2 mrad for reasons similar to those discussed above for the LT.

The OT was optical head was mounted on a D300 Directed Perceptions two-axis gimbal and an Optics in Motion fast steering mirror was used for fine pointing control of the received beam. The actuators and sensors on the OT were controlled with a compact PXI real time processor running LabView.

Initial link demonstrations were performed using the fields of view shown in Table 3. Although the link performed satisfactorily, there were occasional data stream interruptions thought to be associated with occasional, large pointing errors possibly caused by imperfections in the OT gimbal. Subsequent tests performed with $\pm$ 0.5° fields of view were not troubled by these interruptions.

Figure 8 shows a photograph of the OT assembly on the gimbal alongside the instrument rack that houses the lasers, processors, power supplies and receiving and transmitting electronics.

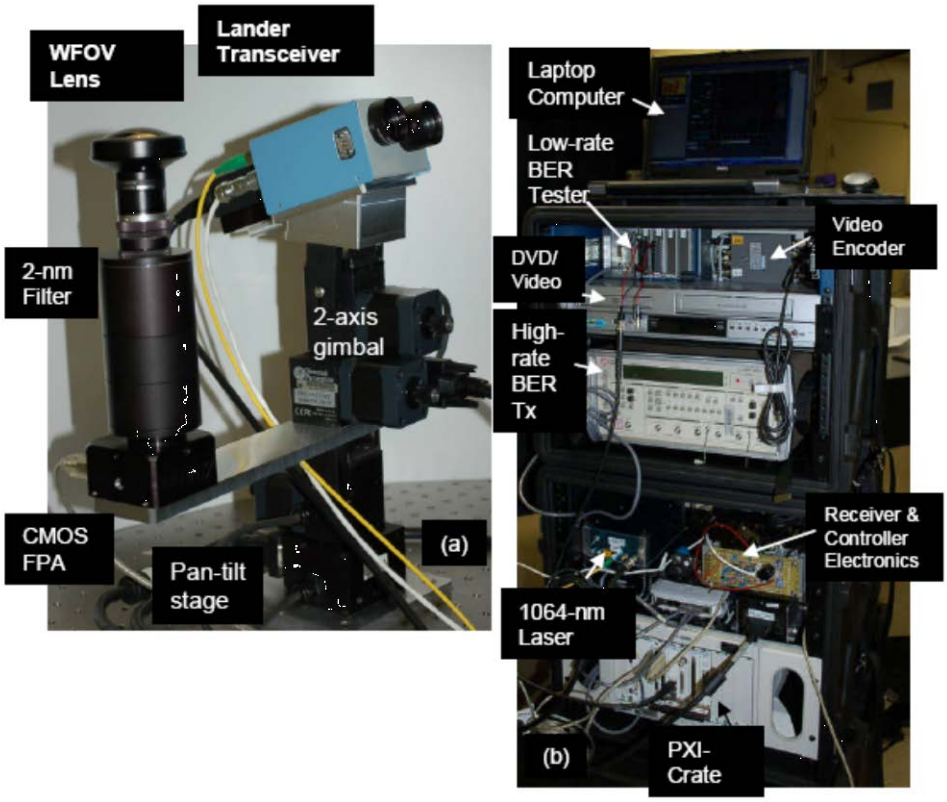

Figure 7. *(a) Lander transceiver comprising a Wide field of View (WFOV) lens camera and micro-stepper motorized 2-axis gimbal camera, with the entire assembly on a pan-tilt stage (b) Instrument rack that includes the laser transmitter, the real-time processor housed in a PXI crate, and data transmitting and receiving electronics*

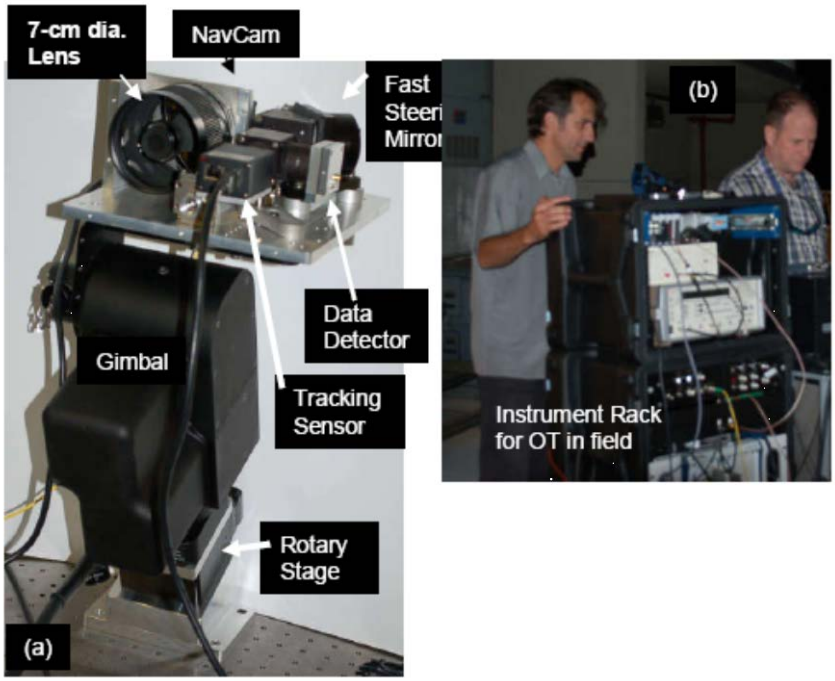

Figure 8. *(a) Orbiter transceiver comprising a 7-cm diameter lens navigation camera and separate optical channels for a data detector controlled by a tracking sensor and fast steering mirror combination. The assembly is mounted on a 2-axis gimbal that is shown mounted on a rotary stage for induced angular slewing. (b) Instrument rack that includes the laser transmitter, real-time processor housed in a PXI crate and data transmitting and receiving electronics.*

4. PROTOTYPE LINK

The prototype transceivers described were used for proof-of-concept testing of the access link acquisition, tracking and bi-directional data transfer. The tests described were conducted on the grounds of the Jet Propulsion Laboratory (JPL) in Pasadena. JPL's main campus is sited on the side of a relatively steep hill, including a peak of approximately 2000 foot elevation known as the "mesa," on which we set up one transceiver of the prototype link. Many of the buildings on the JPL campus are visible from the mesa; the roof of one of these, Building 238, was chosen as the location of the other transceiver (Figure 9).

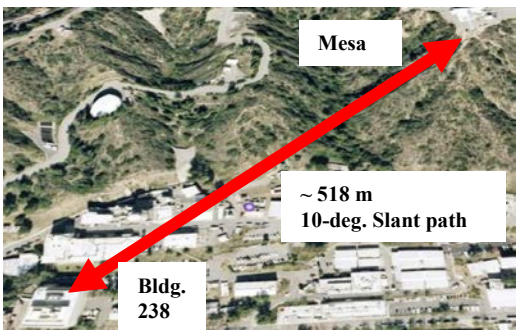

Figure 9: The link used with the prototype transceivers is shown by a red line on the aerial image. The link distance is 500 m over an atmospheric path.

Setup for simulating orbiter overflight

During a Mars access link pass in which the orbiter overflies the lander, the lander will likely be stationary, so the lander transceiver pointing will need to change to follow the orbiter as it passes overhead. Moreover, the attitude of the orbiter may be fixed in inertial space, or constrained by other requirements such as the orientation of solar cells, so that it may be impractical to require the orbiting spacecraft to maintain a constant attitude with respect to the direction to the lander. As a result, motion of the pointing control systems in both transceivers will likely be required to keep the transceivers aimed at each other. Also as a result of the relative motion, the motion-detection algorithm in the lander transceiver's acquisition system will be able to take advantage of the motion of the orbiter across the Martian sky.

This relative motion is difficult to produce directly in a ground-based test such as the one set up at JPL. To simulate the relative motion, the prototype lander transceiver gimbal and the prototype orbiter transceiver gimbal were each mounted on a similar gimbal, which was then driven to simulate the relative motion of orbiter and lander in an access link. Slew rates between 0.5 to 2 degrees / second were typically used. These rates exceed those corresponding to access link conditions but smooth, lower rate slews are difficult to generate using the commercial gimbals in the prototype link.

In the case of the prototype lander transceiver, the lander transceiver gimbal and the lander transceiver acquisition camera were mounted side-by-side on an aluminum plate which was then mounted on the lower gimbal. See Figure 10.

Figure 10: Prototype lander transceiver mounted on gimbal simulating motion of the orbiter transceiver

Likewise the orbital transceiver test configuration is shown in Figure 11.

Figure 11 Prototype orbiter transceiver mounted on a second gimbal during link emulation tests.

During link demonstration tests at JPL, acquisition, pointing control, and optical data transmission were demonstrated. Pointing acquisition was accomplished by first aiming the prototype orbiter transceiver at the prototype lander transceiver, to simulate the latter's illumination by blind pointing of the former. The remainder the acquisition process was automated: the orbiter transceiver's beam was easily detected by the lander transceiver's acquisition camera, and the lander transceiver then locked onto the orbiter transceiver's beam, and illuminated the orbiter transceiver, which then also locked onto the beam it received. Figure 12 shows azimuth (a) and elevation (b) motion of the lander transceiver gimbal, as it moves to track

out simulated orbiter transceiver motion, introduced by the lower gimbal on which the lander transceiver gimbal and acquisition camera are mounted. Figure 12c shows the simulated motion of the orbiter transceiver as seen by the lander transceiver acquisition camera.

Figure 13 shows the tracking errors recorded in the lander transceiver, with 1-σ errors of 125 μrad and 118 μrad in the x (azimuth) and y (elevation) degrees of freedom, respectively. Figure 14 shows similar performance histograms for the orbiter transceiver, showing somewhat better performance than in the lander transceiver. Pointing performance at both ends was sufficiently good to achieve reliable communication with 1 mrad beams, although the beams used in the demonstration had widths of 2 mrad. In particular, these pointing errors would result in pointing loss exceeding the 3.5 dB allocation 99 % of the time in the transmission from the OT to the LT, and 96.5% of the time in the reverse transmission; pointing errors would result in only a slight reduction in link capacity.

During the link demonstration tests we demonstrated data transmission in all of the supported data transfer modes, viz., streaming video (270 Mb/s), error-free PRBS (200 Mb/s) from the LT to the OT, and low-rate PRBS (50 Kb/s) from the OT to the LT.

6. CONCLUSION

An optical access link would be ideally suited to the task of returning high-rate digital data containing high-resolution images from the surface of Mars to a relay satellite in orbit around Mars. In such an access link, the range is sufficiently small that only moderately high precision pointing is needed, so that the pointing control systems could be made relatively simple, light, and inexpensive. We have constructed a prototype of such a system, which uses only a motorized gimbal for pointing control in the lander transceiver, and a motorized gimbal together with a fine steering mirror in the orbiter transceiver. Using these prototypes, we have demonstrated sub-milliradian pointing performance, and the transmission of digitized streaming video at a data rate of 270 Mb/s. Key ongoing developments planned are to make the initial blind-pointing more reliable and to build a larger entrance aperture diameter WFOV camera. We also plan to identify space qualified parts that could be used in future transceiver designs.

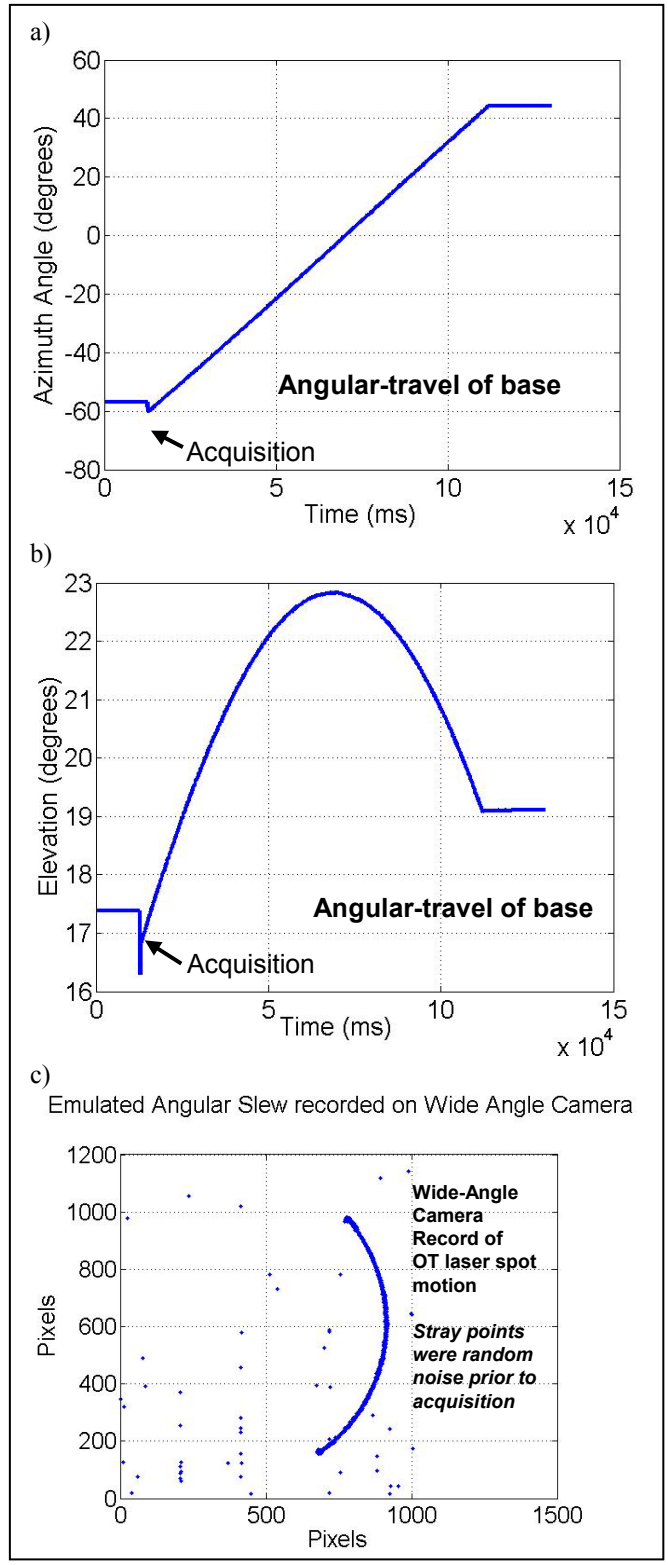

Figure 12: Prototype link data acquired with LT (a) Azimuth axis motion of gimbal (b) Elevation axis motion of gimbal (c) Centroid of OT beacon moving on the WFOV camera.

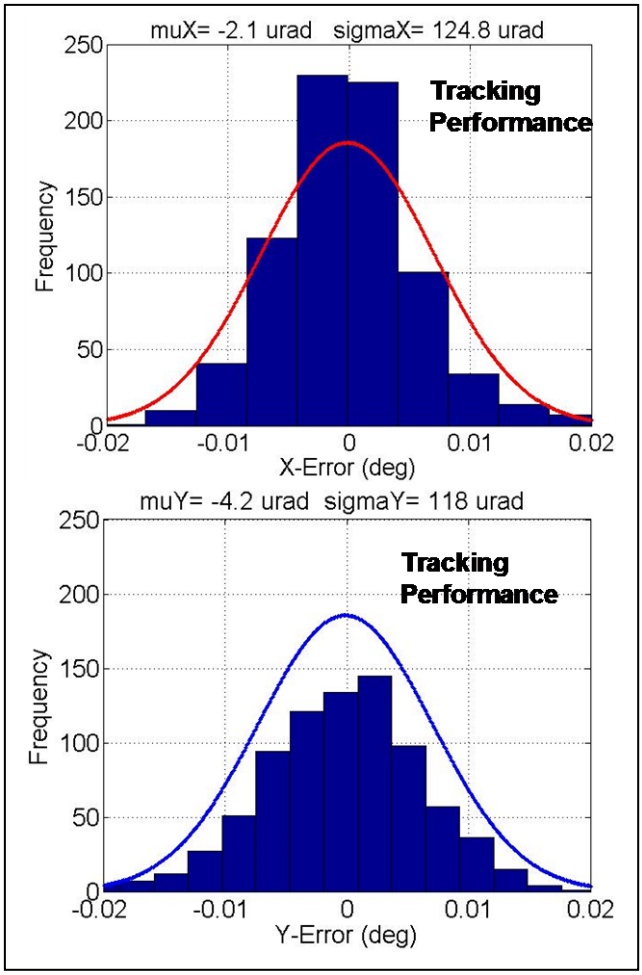

Figure 13: Prototype lander transceiver tracking errors

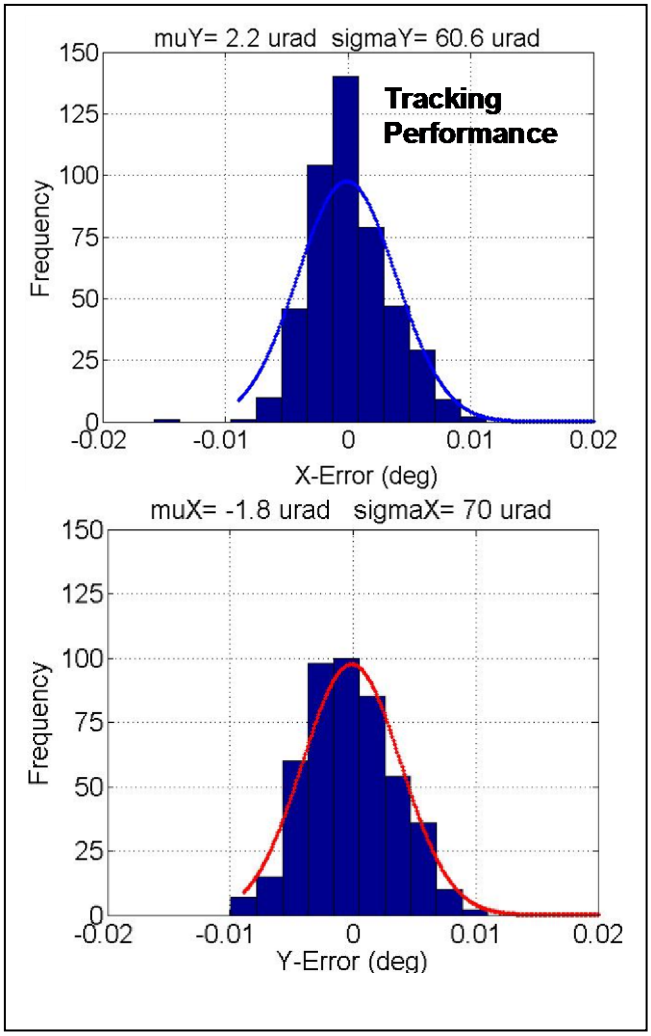

Figure 14: Prototype orbiter transceiver pointing errors

ACKNOWLEDGEMENTS

The research described in this paper was carried out at the Jet Propulsion Laboratory, California Institute of Technology, under a contract with the National Aeronautics and Space Administration. The authors gratefully acknowledge contributions by Kevin Birnbaum Jeffrey Charles, Carlos Esproles, Malcolm Wright, Vachik Garkanian and David Zhu toward development and testing of components and support during link emulations.

REFERENCES

[1] Kjartan M. Kinch, Jascha Sohl-Dickstein, James F. Bell III, R. Johnson, Walter Goetz and Geoffrey A. Landis, "Dust Deposition on the Mars Exploration Rover Panoramic Camera (Pancam) calibration Targets, Journal of Geophysical Research, Vol 112 E06S03, doi:10.1029/2006JE002807, 2007.

[2] M. T. Lemmon , M. J. Wolff, M. D. Smith, R. T. Clancy, D. Banfield, G. A. Landis, A. Ghosh, P. H. Smith, N. Spanovich, B. Whitney, R. Greeley, S. Thompson, J. F. Bell III, W. W. Squyres, " Atmospheric Imaging Results from the Mars Exploration Rovers: Spirit and Opportunity, " Science, Vol. 306, 1753-1756, 2004.

[3] Gregory R. Osche, "Optical Detection Theory for Laser Applications, " Wiley Series in Pure and Applied Optics [Ed. Bahaa E. A. Saleh], 58, 2002.

BIOGRAPHIES

Martin Regehr is a senior engineer at JPL. At JPL, he has participated in the construction of several SIM testbeds, worked on the Formation Control Testbed, and has assisted with optical communications development. He holds a BASc from the University of Toronto and a Ph.D. from Caltech.

Joseph Kovalik received his B.Sc. in physics from the California Institute of Technology and his PhD in physics from the Massachusetts Institute of Technology. He has designed, built and implemented optical communications and metrology systems both at JPL and other national labs. This includes experience with acquisition and tracking of moving objects in order to establish communications links and perform ranging measurements.

Abhijit Biswas is senior engineer at the Jet Propulsion Laboratory working on optical communications for the past 11 years. He has a bachelors degree in Metallurgical Engineering from the Indian Institute of Technology, Kharagpur and a Ph. D. in Molecular Science from Southern Illinois University, Carbondale, IL.